

## Irradiation test in HANARO for neutron absorbing and burnable poison materials

Byung-Ho LEE, Han-Soo KIM, Jong-Man PARK, Jin-Sik CHEON, Je-Yong OH,  
Yang-Hyun KOO, Jeong-Sik YIM, Dong-Seong SOHN  
Korea Atomic Energy Research Institute

### ABSTRACT

$Dy_xTi_yO_z$  and  $Gd_xTi_yO_z$  have been developed as neutron absorbing and burnable poison materials. The  $Dy_xTi_yO_z$  and  $Gd_xTi_yO_z$  were irradiated in the HANARO reactor for a feasibility study and their PIEs were performed to evaluate the in-pile behaviors. The irradiation was successfully performed for 46 EFPD. The PIE results proved to maintain geometrical and microstructural integrity during irradiation. Inductively coupled plasma mass spectrometry (ICP-MS) confirmed the higher depletion rate in  $Gd_xTi_yO_z$  than in  $Dy_xTi_yO_z$ . The irradiation test with PIEs would suggest  $Dy_xTi_yO_z$  and  $Gd_xTi_yO_z$  can be applied for neutron absorbing and burnable poison materials.

### 1. Introduction

The  $Dy_xTi_yO_z$  and  $Gd_xTi_yO_z$  have been developed as neutron absorbing and burnable poison materials. These lanthanoid ( $Ln_2O_3 + MO_2$ ) oxide have been considered as good irradiation resistant materials [1].

The  $Dy_xTi_yO_z$  has been used as control rod material in the VVER-1000 reactors as well as in the research reactors in Russia. The  $Gd_xTi_yO_z$  is being considered as burnable poison material to control the excessive reactivity, provide the safety shutdown margin, and compensate the reducing reactivity.

The present paper describes the irradiation test including an analysis of in-pile behavior for neutron absorbing and burnable poison materials in the HANARO reactor. In addition, PIE results along with chemical analysis are discussed.

### 2. Material fabrication and irradiation capsule

$Dy_2O_3$  and  $TiO_2$  powders were prepared for the fabrication of  $Dy_xTi_yO_z$  pellet.  $Dy_2O_3$  and  $TiO_2$  were well mixed in the tubular mixer and then milled in the zirconia crucible. The green pellet was made following hydraulically pressing the mixed powder under 300 MPa. Based on TMA sinterability scoping tests, the green pellets were sintered at the temperature of 1550 and 1600°C at the atmosphere

of argon [2].

On the other hand, the  $Gd_xTi_yO_z$  pellets were fabricated by very similar procedures as for  $Dy_xTi_yO_z$ . The only difference was sintering temperature, which was 1500 and 1550°C for  $Gd_xTi_yO_z$  instead of 1550 and 1600°C for  $Dy_xTi_yO_z$ .

The prepared pellets were loaded into the irradiation capsule (see Fig. 1). The main characteristics of pellets with designation are listed below.

Pellet	Designation	Height (mm)	Diameter (mm)	Density (g/cc)
$Dy_xTi_yO_z$ (1600 )	DY-HT	7.685	8.525	6.65
	DY-HB	9.112	8.525	6.65
$Dy_xTi_yO_z$ (1550 )	DY-LT	7.428	8.524	6.33
	DY-LB	7.436	8.524	6.28
$Gd_xTi_yO_z$ (1650 )	GD-HT	7.941	8.514	6.27
	GD-HB	8.115	8.514	6.27
$Gd_xTi_yO_z$ (1600 )	GD-LT	8.898	8.521	6.05
	GD-LB	8.848	8.521	6.04

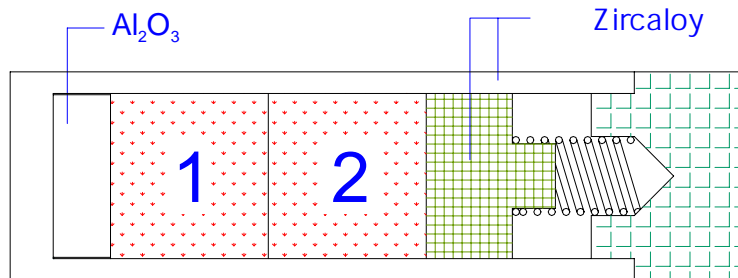


**Fig. 1. Pellet capsule for HANARO test**

### 3. Irradiation test and in-pile analysis

The  $Dy_xTi_yO_z$  and  $Gd_xTi_yO_z$  were irradiated to test their applicability to neutron absorbing and burnable poison materials. The irradiation was performed in the HANARO research reactor.

The position of the capsule in the reactor was OR6 throughout the irradiation test. The irradiation period was from July 2001 to October 2001 for 46 EFPD. This test aimed to check the in-pile performance for the first manufactured candidate materials, so irradiation period was shorter than the required testing period.

Before loading into test reactor, the preliminary analyses were performed to estimate the irradiation conditions. In particular, the thermal and stress and strain behaviors were estimated by ABAQUS code with following assumptions:

- ◆ The axial symmetry is applied for the modeling of pellet and cladding due to the geometrical symmetry.
- ◆ Axial heat transfer is negligible.
- ◆ Radiation heat transfer can be neglected through gap between absorbing pellet and cladding. Only gap conductance is considered.

The thermal conductivity was measured by using the laser flash method before irradiation test.  $Dy_xTi_yO_z$  shows the almost constant thermal conductivity with temperature whereas  $Gd_xTi_yO_z$  varies considerably with temperature.

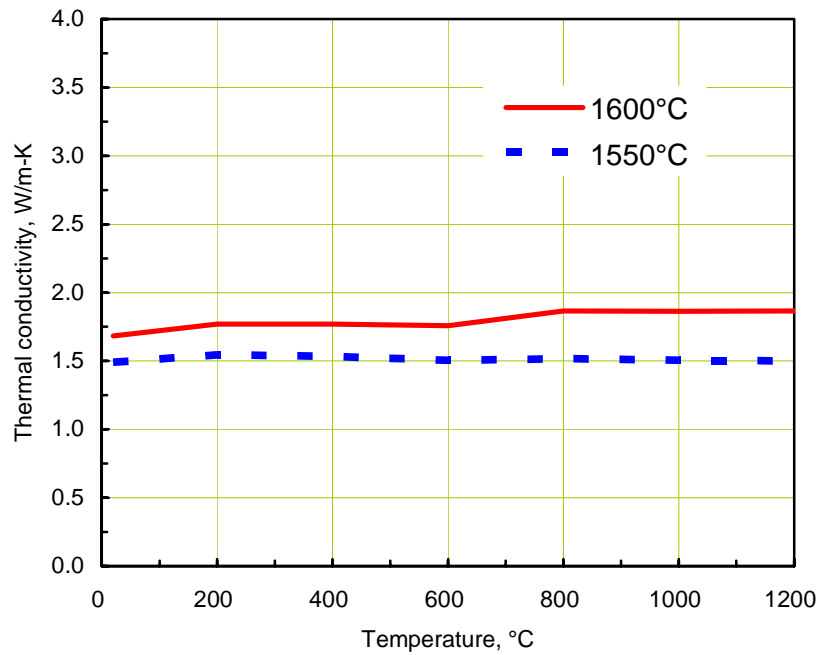


**Fig. 2. Thermal conductivity measured for  $Dy_xTi_yO_z$ .**

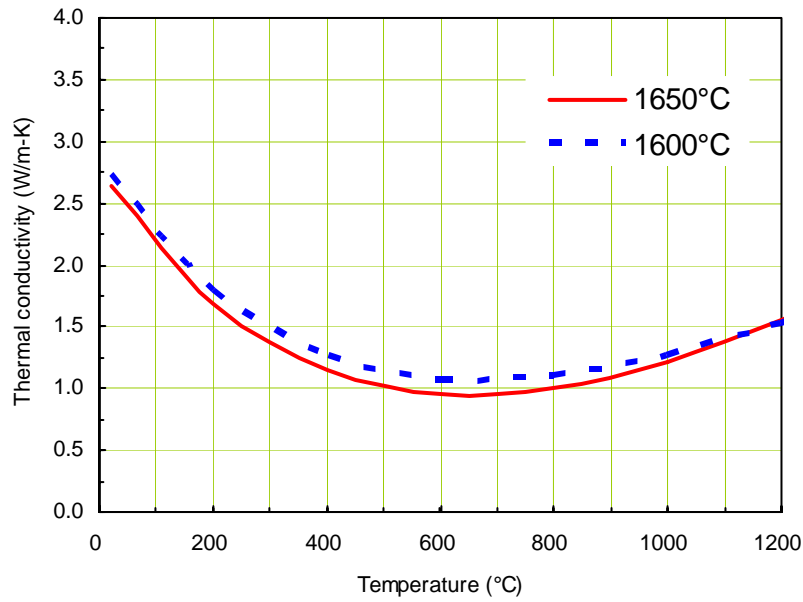


**Fig. 3. Thermal conductivity measured for  $Gd_xTi_yO_z$ .**

The thermal conductivity of  $Dy_xTi_yO_z$  ranges from 1.5 to 2.0 W/m-K and remains almost constant with temperature. The higher sintering temperature – the higher density – results in the higher thermal conductivity of  $Dy_xTi_yO_z$ .

On the other hand, the thermal conductivity of  $Gd_xTi_yO_z$  decreases with temperature up to 600°C and then increases with temperature. It is noticeable that the sintering temperature effect is fairly insignificant in the thermal conductivity.

For the simplicity of calculation and the conservatism, the thermal conductivity of 1.5 and 1.0 W/m-K was applied for  $Dy_xTi_yO_z$  and  $Gd_xTi_yO_z$ , respectively.

The Ross and Stoute model [3] was used for the gap conductance between a pellet and cladding. The gap was charged with He gas of 1 bar at the room temperature. The conduction by He gas was taken into account and its value is 0.2 kW/m-K for thermal conductivity with the assumption of the surface roughness of 1  $\mu\text{m}$ .

The Dittus-Boelter relationship was used for heat transfer from the coolant to cladding. The pellet centerline temperature was estimated with no swelling for conservatism. The linear heating rate was 108 W/cm for  $Dy_xTi_yO_z$  and 172 W/cm for  $Gd_xTi_yO_z$ .

Taking in account the coolant conditions, gap properties, heat generation, the calculated centerline temperature in  $Dy_xTi_yO_z$  sintered at 1600 was ~600 and 700 with power depression and uniform power distribution, respectively. In the case of  $Gd_xTi_yO_z$  sintered at 1650, the thermal analysis results to ~1150 and 1500 with power depression and uniform power distribution, respectively.

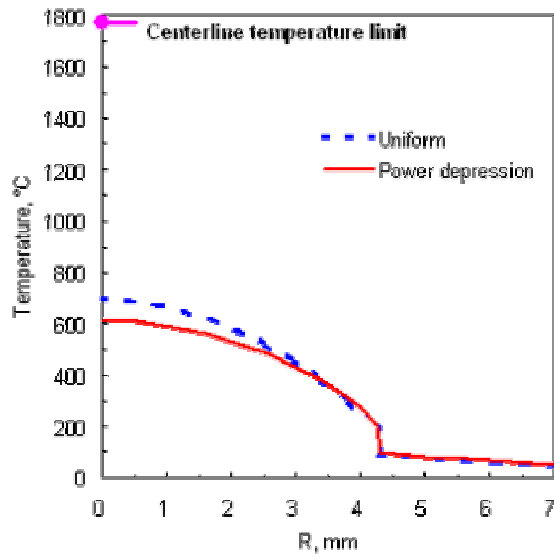


Fig. 4. The radial temperature distribution for  $Dy_xTi_yO_z$ .

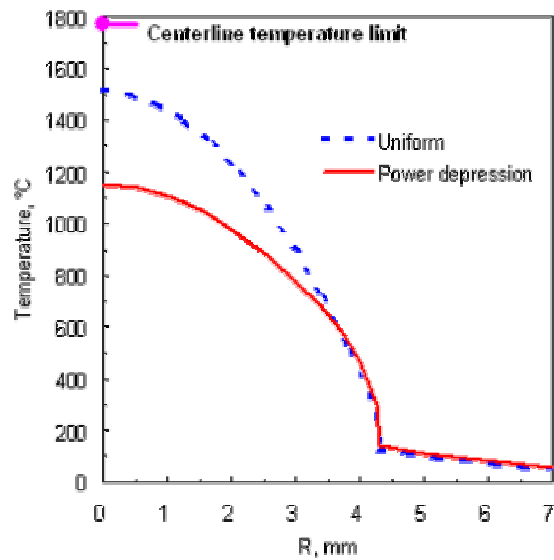


Fig. 5. The radial temperature distribution for  $Gd_xTi_yO_z$ .

The stress and strain analysis revealed that there is no contact between the pellet and capsule cladding (Zircaloy-4).

## 4. Post Irradiation Examination

### 4.1 Geometry and Density

The density of  $Dy_xTi_yO_z$  and  $Gd_xTi_yO_z$  after irradiation was measured for the changes in the pellets.

The diameter and height were also measured. The pellet changes can result from the in-reactor sintering and swelling from the presence of solid fission products and/or from the precipitation of gaseous fission products into pores.

The immersion density measurements were performed on eight specimens. The weight measurements were repeated five times to obtain reliable and consistent average values. Results of density together with diameter and height measurements were summarized below:

Pellet	Designation	Height (mm)	Diameter (mm)	Density (g/cc)
Dy <sub>x</sub> Ti <sub>y</sub> O <sub>z</sub> (1600 )	DY-HT	7.681	8.505	6.68
	DY-HB	9.122	8.533	6.68
Dy <sub>x</sub> Ti <sub>y</sub> O <sub>z</sub> (1550 )	DY-LT	7.436	8.552	6.81
	DY-LB	7.437	8.526	6.78
Gd <sub>x</sub> Ti <sub>y</sub> O <sub>z</sub> (1650 )	GD-HT	7.947	8.520	6.43
	GD-HB	8.116	8.515	6.45
Gd <sub>x</sub> Ti <sub>y</sub> O <sub>z</sub> (1600 )	GD-LT	8.881	8.521	6.36
	GD-LB	8.914	8.520	6.37

However, the open porosity in the specimens was not properly treated due to the limited equipment in the hot cell. To take into account the open porosity, the following additional estimation was applied to compensate the open porosity in the pellet.

$$\rho_x = \frac{w_{air}}{w_{air} \left( 1 + \frac{P \cdot \rho_l}{\rho_x} \right) - w_l} \cdot \rho_l$$

where  $\rho_x$  and  $\rho_l$  are the density of specimen and liquid, and  $w_{air}$  and  $w_l$  are the weight in the air and in the liquid. P is porosity in the pellet.

Based on the observation of OM, the adequate porosity was assumed and the iterative calculation was made to obtain the corrected density. Hence, the volume change was estimated by using the following relationship between the density before and after irradiation.

$$\frac{V - V_0}{V_0} \Big|_{dens,swell} \approx \left( 1 - \frac{\rho_x}{\rho_0} \right)$$

The calculated volume change is shown in Fig. 6 and Fig. 7. The squares in the figures include the values for the pellets with appropriate porosity.

The DY-H (sintered at the higher temperature) indicates significant swelling whereas there is no volume change or slight swelling in DY-L. On the other hand, both Gd<sub>x</sub>Ti<sub>y</sub>O<sub>z</sub> pellets shows slight

swelling.

To obtain more accurate in-pile volume behaviors, it is required to improve the density measuring system in the hot cell and to prepare more sophisticated porosity data before irradiation.

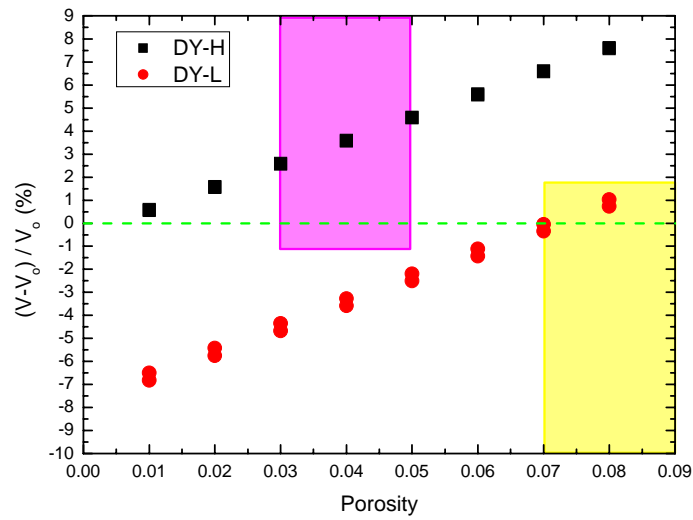


Fig. 6. The density changes depending on porosity for  $Dy_xTi_yO_z$ .

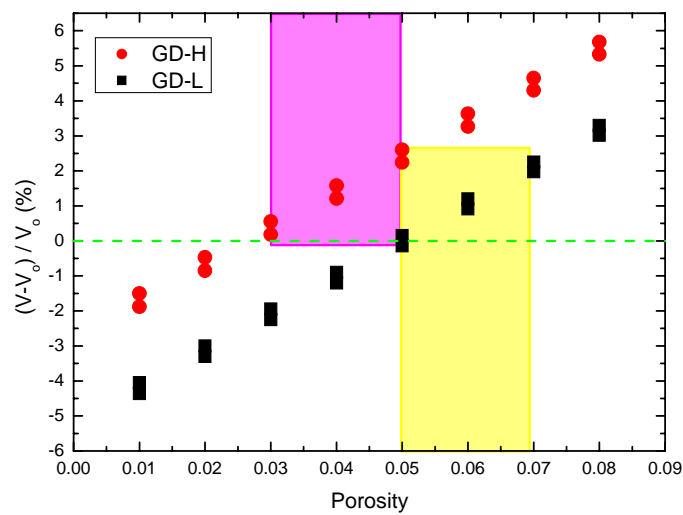
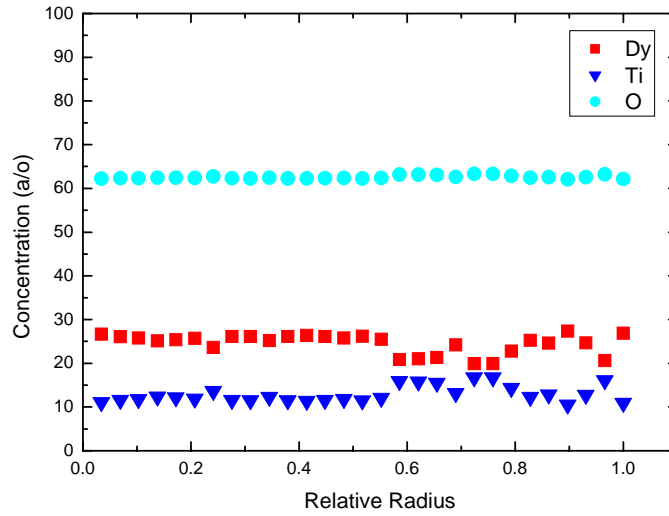


Fig. 7. The density changes depending on porosity for  $Gd_xTi_yO_z$ .

#### 4.2 EPMA

The EPMA measurements were made for DY-HB and GD-LB after irradiation. The quantitative measurements were performed along the radius from the pellet center to periphery to obtain the radial

profiles of Dy, Gd, Ti, and O concentration in candidate material.



**Fig. 8. Radial profile of Dy, Ti, and O concentrations in  $Dy_xTi_yO_z$**

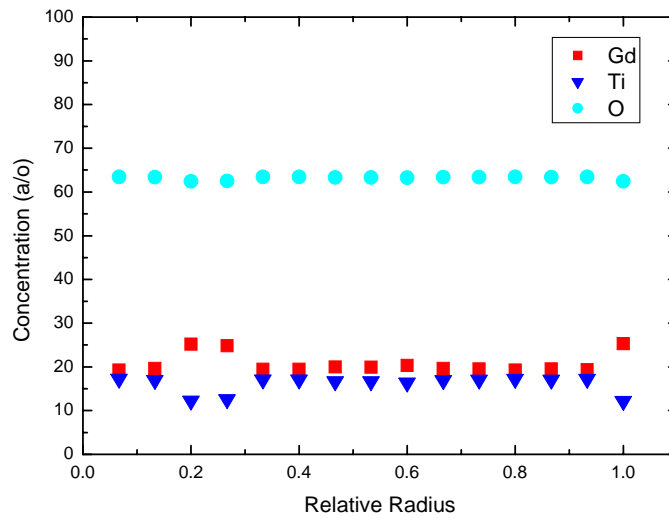


**Fig. 9. Radial profile of Gd, Ti, and O concentrations for  $Gd_xTi_yO_z$**

The radial profiles were presented for  $Dy_xTi_yO_z$  in Fig. 8 and for  $Gd_xTi_yO_z$  in Fig. 9. The points of 29 and 15 were used for  $Dy_xTi_yO_z$  and for  $Gd_xTi_yO_z$ , respectively. In the figures, it can be seen that the oxygen distributes very uniformly along the radius whereas the Dy and Gd concentrations vary along the radius. The variation seems to be attributed to the non-uniformity of Dy and Gy.  $Dy_xTi_yO_z$  consists of  $Dy_2TiO_5 + Dy_2Ti_2O_7$ . The non-uniformity indicates the variation of two phases in the  $Dy_xTi_yO_z$  pellet and in same way in  $Gd_xTi_yO_z$ . Nevertheless, it can be assured that there is no macroscopic migration of Dy and Gd during irradiation. Consequently, it is expected that developed

materials function well in the reactor.

### 4.3 Chemical Analysis

Inductively coupled plasma mass spectrometry (ICP-MS) was applied to estimate the absorbing elements depletion due to irradiation [4]. The depletion was measured for DY-HT and GD-HB. The changes in neutron absorbing isotopes are presented in Fig. 10 for  $Dy_xTi_yO_z$  and Fig. 11 for  $Gd_xTi_yO_z$ . The important isotopes having rather high thermal neutron absorption cross-sections are Dy-164(2700 barn) for  $Dy_xTi_yO_z$  and Gd-155(61,000 barn) and Gd-157(254,000 barn) for  $Gd_xTi_yO_z$ .

Decay products of Dy-164 are Ho and Er. However the only Ho-165 was detected since the produced amount of Er was less than that required for accurate measurement. The amount of Ho produced is slightly larger than that of Dy-164, which means the Dy-164 was produced by chain reaction along with consuming by neutron absorption. This fact confirmed that the efficiency of  $Dy_xTi_yO_z$  decreases at a slow rate rather than the other neutron absorption candidate for control rod, for example,  $B_4C$ .

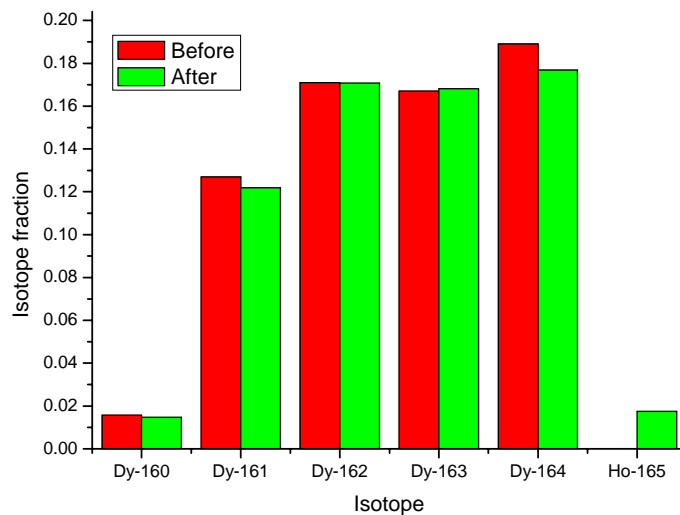


**Fig. 10. Isotope changes in  $Dy_xTi_yO_z$  due to irradiation.**

On the other hand, the Gd-155 and Gd-157 depleted more than 50% after irradiation (Fig. 11). The higher depletion in  $Gd_xTi_yO_z$  than in  $Dy_xTi_yO_z$  results from the negligible neutron absorption of Gd isotopes except the Gd-155 and Gd-157. The Gd-155 and Gd-157 transmute to Gd-156 and Gd-157 very quickly with irradiation whereas the neutron absorption by Gd-156 and Gd-157 is very negligible due to their very low neutron absorption cross section.

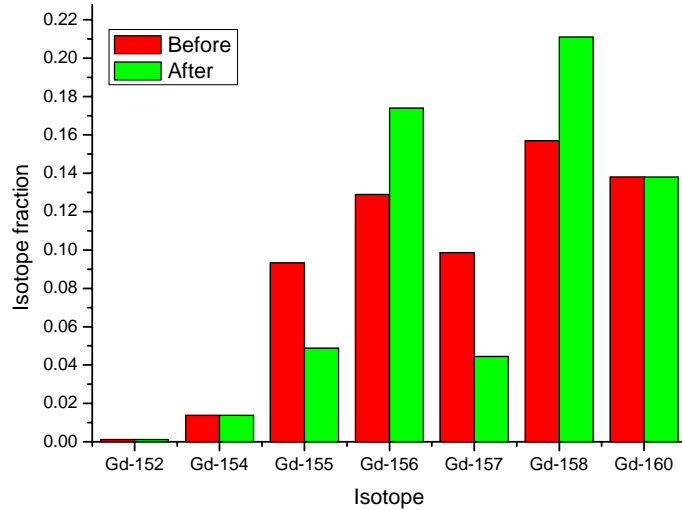


**Fig. 11. Isotope changes in  $Gd_xTi_yO_z$  due to irradiation.**

## 5. Conclusion

The  $Dy_xTi_yO_z$  and  $Gd_xTi_yO_z$  were irradiated in the HANARO reactor to evaluate the in-pile performance as a feasibility study for neutron absorbing and burnable poison materials. The irradiation for 46 EFPD was successful and the PIE results indicate the in-pile performance with stable geometrical and microstructural integrity. Inductively coupled plasma mass spectrometry (ICP-MS) confirmed the higher depletion rate in  $Gd_xTi_yO_z$  than in  $Dy_xTi_yO_z$ .

## Acknowledgement

The authors would like to express their appreciation to the Ministry of Science and Technology (MOST) of the Republic of Korea for the support of this work through the mid- and long-term nuclear R&D Project. We also acknowledge many staffs in HANARO team, IMEF and CAF who performed the HANARO operation, nuclear physics calculation, PIE and chemical analysis. We wish to thank Dr. S.H. Lee (KRISS) for measuring the thermal conductivity.

## Reference

- [1] V.D. Risovany, E.E. Varlashova, D.N. Suslov, "Dysprosium Titanate as an Absorber Material for Control Rods", *Journal of Nuclear Materials*, Vol. 281 (2000) 84-89.
- [2] H.S. Kim, et al., "Study on the sinterability and pellet properties of  $Dy_2O_3$ - $TiO_2$  oxide", *J. Kor. Cer. Soc.* 39, 2002, p1108.
- [3] A.M. Ross, R.L. Stoute, "Heat Transfer Coefficient Between  $UO_2$  and Zircaloy-2", CRFD 1075/AEC 1952, 1962.
- [4] J.K. Kim, private communication, 2003.